A 77-GHz FMCW MIMO Radar Employing a Non-Uniform 2D Antenna Array and Substrate Integrated Waveguides

Simon P. Hehenberger
Communications and RF Systems
Johannes Kepler University Linz
Linz, Austria
simon.hehenberger@jku.at

Alexander Yarovoy
Microwave Sensing, Signals and Systems
Delft University of Technology
Delft, Netherlands
a.yarovoy@tudelft.nl

Andreas Stelzer
Communications and RF Systems
Johannes Kepler University Linz
Linz, Austria
andreas.stelzer@jku.at

***Abstract*—In state-of-the-art frequency-modulated continuous-wave (FMCW) multiple-input multiple-output (MIMO) radar systems, antennas are usually designed based on microstrip technology. They are arranged in uniform arrays such that the synthesized virtual array maximizes the angular resolution. This paper presents the design of a 77-GHz FMCW MIMO radar frontend with antennas and feed structures based on substrate integrated waveguides (SIW) and non-uniform planar arrays optimized for sidelobe suppression. A design procedure for MIMO arrays with particular emphasis on sidelobe level suppression based on convex optimization is presented, and a novel transition from differential microstrip line to SIW is utilized to feed the transmit antennas. Measurements show the successful SIW and antenna design, as well as a sidelobe level of −40 dB within the field of view (FOV) of the radar system.**

***Index Terms*—Array processing, FMCW radar, MIMO radar, radar system, slot array antenna, antenna design, substrate integrated waveguide (SIW), waveguide transitions**

I. Introduction

State of the art automotive radar systems employ low-cost, fully-integrated, multi-channel radar circuits mounted on a low loss substrate, which also shelters transmit and receive antennas, respectively. The utilized radiators are most commonly manufactured using microstrip technology and are arranged in uniform arrays such that the synthesized virtual array maximizes the angular resolution of the system. In order to satisfy the spatial sampling theorem, it is necessary that the spacing between individual elements does not exceed $\lambda/2$, with λ denoting the free-space wavelength, which leads to a considerable number of channels and high cost. The spatial-aliasing effect can be mitigated by employing non-uniform arrays. Furthermore, the angular resolution, as well as the dynamic range, or sidelobe level (SLL) of the system, can be manipulated by the application of so-called spatial density tapers [1]. If the system permits a limited field of view (FOV), the sampling requirements can be further relaxed by allowing grating lobes outside of the systems FOV.

Antennas in microstrip form are easy and cheap to manufacture but also show drawbacks like unwanted radiation from the feed lines, low bandwidth, and severe coupling to adjacent elements. The substrate integrated waveguide (SIW) approximates the behavior of a rectangular waveguide (RWG) and mitigates the effect of line radiation and coupling to adjacent elements. Despite the benefits of the SIW, it's application is still uncommon due to its bulkiness and lack of suitable transitions to commonly employed MMIC packages. This paper is structured as follows. First, the design of the SIW, suitable transitions from MMICs to the SIW, the antenna element, and the array topology are discussed. Section 3 presents the experimental verification of the SIW, the antenna, and the whole system.

II. Radar System Design

The radar system with $N_{\text{TX}} = 8$ transmit and $N_{\text{RX}} = 16$ receive channels is built upon the 77 GHz radar chipset from Infineon. The three-channel transmitter RTN7735 is used for FMCW waveform generation, and the signal is distributed to the transmit antennas by means of RPN7720 digital power amplifiers and digital control signals.

A. Waveguide and MMIC Transitions

The design parameters of the SIW, as sketched in Fig. 1 a) are the substrate height b and permittivity ε_r, the metallized through-hole diameter d_{via}, the distance between two consecutive metallized through holes p_{via} as well as the distance between the parallel rows of vias a. The design was carried out on a predefined layer-stack, with Rogers RO3003 substrate, which eliminated the height of the substrate b as a design parameter. Furthermore, a ratio of d_{via} and p_{via} that promised simple manufacturing and good yield was chosen. The SIW is modeled by assuming an equivalent rectangular waveguide with dimensions a_{RWG} and $b_{\text{RWG}} = b$ that obtains the same cut-off frequency and propagation behaviour as the SIW [2]. The cut-off frequency of the equivalent waveguide is chosen such that the frequency of operation is roughly a factor 1.4 higher than the cut-off, which promises low reflections and negligible dispersion. The resulting SIW width a is calculated according to the empirical model introduced in [3], and an overview

978-1-7281-6755-8/20/$31.00 ©2020 IEEE

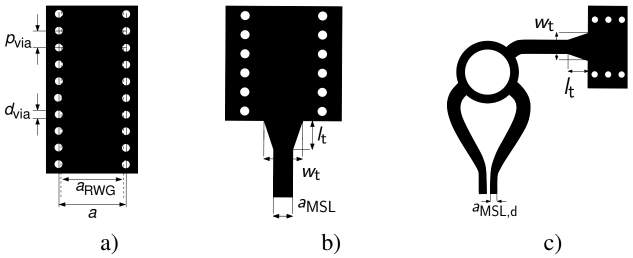

Fig. 1: a) SIW geometry with width of equivalent waveguide a_{RWG}. Single layer transitions from a) single-ended and b) differential microstrip to SIW.

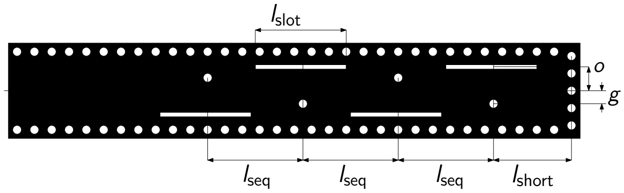

Fig. 2: Design parameters for a resonant array of slots in a SIW spaced l_{seq} apart with a distance of l_{short} from the center of the last slot to the shorted end of the waveguide.

of design parameters and resulting waveguide dimensions are given in Tab. I.

TABLE I: SIW design parameters and resulting dimensions.

ε_r	d_{via}	p_{via}	a_{RWG}	a	b
3	200 µm	400 µm	1.57 mm	1.71 mm	127 µm

In order to use the SIW in cooperation with the RPN7720 power amplifier and the RRN7745 receiver, suitable transitions from differential and single-ended microstrip transmission lines need to be designed. This transition is straight-forward when considering single-ended lines. The solution in Fig. 1 b) implements the transition by simply tapering the microstrip line to a width w_t over a length l_t and connecting to the top wall of the SIW as introduced in [4]. The transition from a differential line is not as straight-forward. This work employes a balun, based on a rat-race coupler [5], prior to transitioning into the SIW with the same tapered microstrip section used in the single-ended solution as shown in Fig. 1 c).

B. Antenna

The antenna employed as an individual element in the receive and transmit array respectively is realized as a resonant array of longitudinal slots in a shorted SIW, as sketched in Fig. 2. The spacing between the slots l_{seq} in a resonant array of slots should correspond to half a wavelength of the propagating mode in the waveguide at the design frequency. In order to achieve the desired elevation half-power beamwidth of the antenna $\Theta_{\text{e,req}} = 30°$, $M = 4$ slots with length l_{slot}, width w_{slot} and an offset o from the center of the waveguide are introduced. The individual slots with admittance $Y_{\text{slot,i}} = G_{\text{slot,i}} + jB_{\text{slot,i}},\ i = 1,\ldots,M$ are required to be resonant ($B_{\text{slot,i}} = 0$) at the design frequency and a well-matched antenna requires the normalized slot conductances to satisfy

$$\sum_{i=1}^{M} \frac{G_{\text{slot,i}}}{Y_0} = 1 \tag{1}$$

with Y_0 denoting the admittance of the equivalent rectangular waveguide. For uniformly excited slots the desired slot conductance is $G_{\text{slot,i}} = 1/M = 0.25Y_0$. Although a closed-form expression for the conductance of a resonant slot in a waveguide exists [6], this expression is less justified for waveguides with small heights [7]. To obtain a resonant slot that is matched to the required conductance, as calculated above, an additional degree of freedom is necessary. This additional design parameter is introduced through an inductive post next to the slot, with an offset g from the waveguide center. This approach to match a slot with an inductive post has already been successfully employed in [8]. After a resonant slot with the required conductance at the design frequency is found, M of these slots are introduced into the shorted SIW, giving rise to two problems. The first is that the distance from the center of the last slot to the exact position of the short l_{short} is unknown and second, the slots and inductive posts will slightly disturb the propagation constant in the SIW. To compensate for this a two-step optimization approach is employed. First, the distance between consecutive slots l_{seq} and the short length l_{short} are both subject to an optimization which aims to place the slots at the maxima of the excited standing wave in the waveguide, thus uniformly exciting the individual slots with equal phase at the design frequency. Second, the slot length l_{slot}, slot offset o and via offset g are subject to an optimization that minimizes the reflection coefficient at the design frequency.

C. Array Topology

Commonly employed planar MIMO array topologies, as discussed in [9], are difficult to manufacture within a single layer of RF substrate due to the resulting complexity of the feeding network. Therefore, in this work, a linear spatial density tapered MIMO array is designed that minimizes the sidelobe level in the azimuth FOV, and a planar array is created by giving individual elements in the transmit array an offset in the orthogonal direction. Although deterministic design algorithms for spatial density tapered arrays exist [10], these algorithms lack the option to consider system parameters like a minimum interelement distance. Therefore, a convex iterative optimization algorithm for the synthesis of uniform amplitude, space tapered linear arrays, as presented in [11], is used to design linear receive and transmit arrays with minimal SLL, respectively. Care is taken that both arrays obtain the same main beamwidth and thus mutually suppress their respective sidelobes in the resulting MIMO two way pattern. For the extension to a planar topology, four elements were chosen and given an offset of $\pm d$. The offset is chosen such that the beamwidth of the array factor in the elevation plane becomes minimal while allowing no grating lobes within the FOV. Fig.

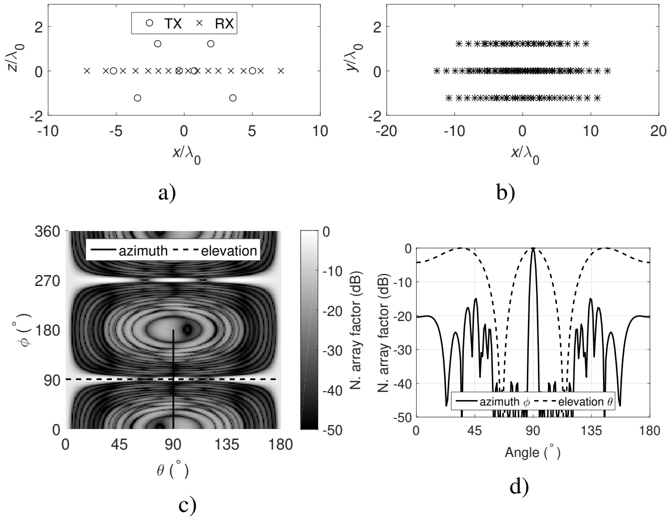

Fig. 3: Array topology, with a) Positions of TX and RX elements, b) synthesized virtual array, and corresponding array factor as c) function of azimuth ϕ and elevation θ angle and d) 1D cuts for $\phi = 90°$ and $\theta = 90°$.

3 a) shows the obtained element positions in the transmit and receive array, respectively, while Fig. 3 b) depicts the positions of the synthesized virtual array elements normalized to the wavelength at the design frequency λ_0. Both, the resulting array factor as a function of azimuth ϕ and elevation θ angle depicted in Fig. 3 c) as well as the 1D cuts for $\phi = 90°$ and $\theta = 90°$ in Fig. 3 d) show a maximal SLL of $-40\,\mathrm{dB}$ within the FOV of the system.

III. Experimental Validation and Discussion

The proper working of individual components, as well as the whole system, was experimentally verified utilizing a wafer prober station and an anechoic chamber.

A. Waveguide Losses and Propagation

The design of the SIW was verfied by extracting its complex propagation constant written as

$$\gamma = \alpha + \mathrm{j}\beta \tag{2}$$

where α is the attenuation constant and β is the phase constant, from the measurements. The measured frequency dependent values for both the attenuation and phase constant are compared to theoretical values obtained through the equivalent waveguide model for both SIW and MSL in Fig. 4 The measured phase constants for both microstrip and SIW are slightly higher than predicted by theory, and while the measured attenuation constant matches the predicted one nicely for the microstrip, for the SIW, the measured one is roughly $0.15\,\mathrm{dB\,cm^{-1}}$ higher than predicted.

B. Antenna Resonance Frequency and Bandwidth

In order to verify the design process of the antenna, three antennas with different design frequencies $f_\mathrm{d} \in \{76.5\ 77\ 77.5\}$ GHz were manufactured. The reflection coefficient of the manufactured antennas has been measured while covering the radiating slots with an absorbing material, and the result is compared to full-wave simulations in Fig. 5. The simulated and measured reflection coefficients of the three antennas compare very well as their resonances are offset only by roughly $500\,\mathrm{MHz}$ for each of the three design frequencies. Detailed results about measured resonance frequency and bandwidth limits of the three antennas are summarized in Tab. II

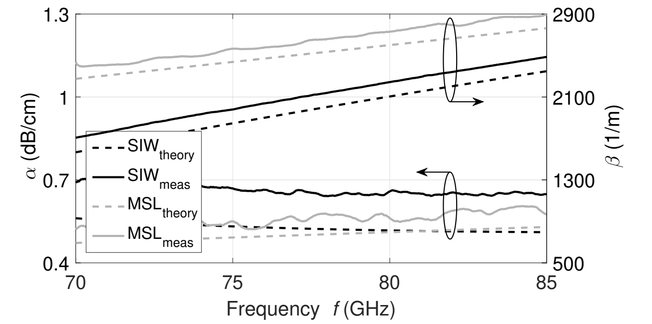

Fig. 4: Comparison of measured and theoretically obtained attenuation α and phase constant β of both an SIW (black) and microstrip line (grey).

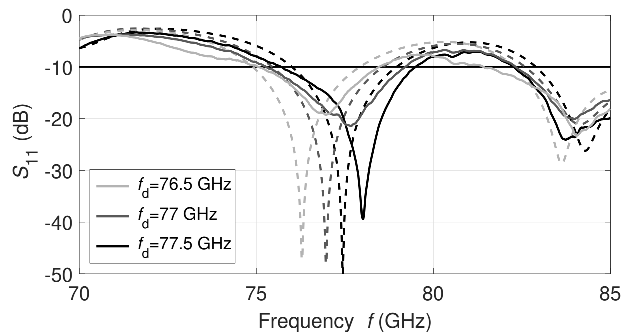

Fig. 5: Reflection coefficient measurement results (solid) for substrate integrated waveguide antenna with four slots and design frequencies $f_\mathrm{d} \in \{76.5\ 77\ 77.5\}$ GHz compared to simulations (dashed).

TABLE II: Comparison between simulated and measured antenna resonance frequencies f_res and bandwidths B_ant for different design frequencies f_d.

f_d	f_res	f_lo	f_up	B_ant
GHz	GHz	GHz	GHz	GHz
76.5	76.96	75.06	78.46	3.40
77	77.68	75.28	79.20	3.92
77.5	78.02	75.72	79.48	3.76

C. Radar System

The following presents measurements that were carried out with the fully assembled system, seen in Fig. 6, with FMCW parameters defined in Tab. III. The individual channel gain and phase errors, as well as the effects introduced by different feed lengths, are compensated through the application of a single target calibration approach.

1) Link Budget: The voltage at the terminals of the ADC resulting from a corner cube (CC) at broadside at a distance of R_t was calculated according to the radar range equation while taking into account the measured losses in the SIW. The mean of the received power over all receive channels is plotted

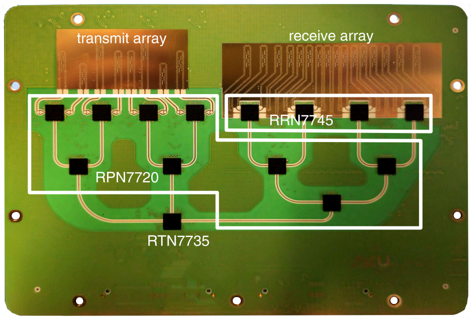

Fig. 6: Manufactured FMCW MIMO frontend built upon the 77 GHz radar chipset from Infineon employing non-uniform transmit and receive arrays with antenna elements based on substrate integrated waveguides.

TABLE III: Summary of the FMCW parameters used to record radar measurements.

Ramp duration	T_c	256	µs
Start frequency	f_0	76	GHz
Chirp bandwidth	B_{chirp}	2	GHz
Number of samples	N_{sample}	1024	

for various active transmit channels as a function of target distance and compared to a theoretical prediction in Fig. 7. It can be seen in Fig. 7 that the measured received power starts to behave according to the prediction for target ranges above $1.5\,\mathrm{m}$, which is the Fraunhofer boundary of the employed CC.

2) Target Measurement: Measurements were performed with two equally sized CCs, placed at equal elevation angles $\theta_{t,1} = \theta_{t,2}$ but different ranges $R_{t,1} \neq R_{t,2}$ and azimuth angles $\phi_{t,1} \neq \phi_{t,2}$. Fig. 8 shows the cuts through the calculated angular spectrum for both target distances and elevation angles normalized to the maximum reflection. When comparing the measured angular spectrum of targets 1 and 2 in Fig 8, it can be seen that the SLL degrades for target angles off broadside. This is due to the simple calibration method applied, which does not take angle-dependent effects or mutual coupling into account.

D. Conclusion

A novel millimeter-wave MIMO system, transmitting linear frequency chirps in the W-band at 77 GHz, usable for 3D positioning, has been presented. The proposed system utilizes

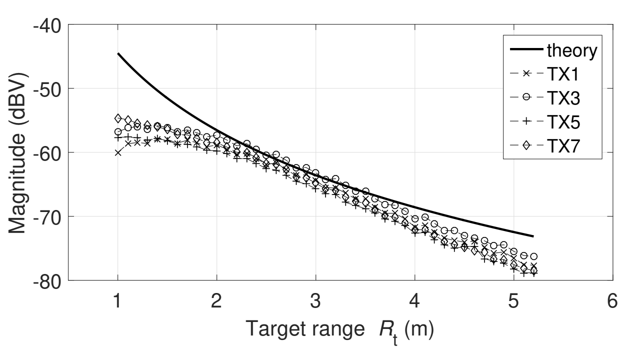

Fig. 7: Link budget of the radar system. Prediction compared to mean measured receive power in all channels for 4 individually active TX channels.

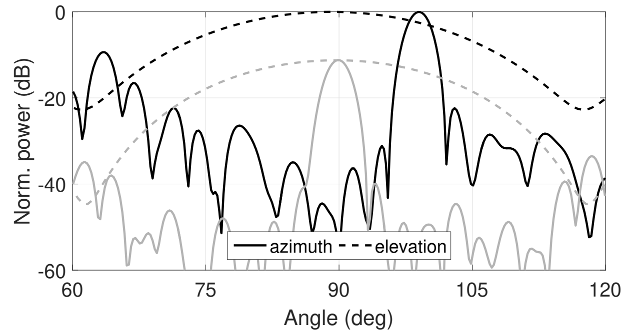

Fig. 8: Azimuth and elevation cut through the calculated angular spectrum for CC 1 (black, $R_{t,1} = 3\,\mathrm{m}$, $\phi_{t,1} = 110°$, $\theta_{t,1} = 90°$) and CC 2 (grey, $R_{t,2} = 5\,\mathrm{m}$, $\phi_{t,2} = 90°$, $\theta_{t,2} = 90°$).

non-uniform antenna arrays designed with an iterative convex optimization algorithm to achieve minimal SLL within the FOV of the radar. Although measurements verified an SLL of roughly $-40\,\mathrm{dB}$ for a target at broadside, sophisticated calibration techniques are necessary to achieve this result also for other target angles. Furthermore, the utilization of non-uniform sampling as a basis for the calculation of the angular spectrum prohibits the use of efficient 2-D FFT based algorithms and thus computationally more expensive. The utilization of SIWs in preference of microstrip technology has to be carefully considered, and although the antenna element, based on a linear array of slots, behaved as expected, the losses in the SIW were higher than predicted. The antenna design complexity, as well as the conductive losses in the SIW, might be reduced by employing a substrate with higher thickness.

References

[1] Willeut, R.E. (1962). Space Tapering of Linear and Planar Arrays.
[2] Y. Cassivi et al. , "Dispersion characteristics of substrate integrated rectangular waveguide," in IEEE Microwave and Wireless Components Letters, vol. 12, no. 9, pp. 333-335, Sept. 2002.
[3] Li Yan et al. Cui, "Simulation and experiment on SIW slot array antennas," in IEEE Microwave and Wireless Components Letters, vol. 14, no. 9, pp. 446-448, Sept. 2004.
[4] D. Deslandes, "Design equations for tapered microstrip-to-Substrate Integrated Waveguide transitions," 2010 IEEE MTT-S International Microwave Symposium, Anaheim, CA, 2010, pp. 704-707.
[5] R. Jungmaier et al., "Rat-race based microstrip coupler with differential port to realize monostatic RF systems," 2012 IEEE/MTT-S International Microwave Symposium Digest, Montreal, QC, 2012, pp. 1-3.
[6] Elliott, R.S.. (2003). Antenna theory & design. 10.1109/9780470544174.
[7] Stern, G.J., & Elliott, R.S. (1985). Resonant length of longitudinal slots and validity of circuit representation: Theory and experiment.
[8] T. Mikulasek et al., "Design of aperture-coupled microstrip patch antenna array fed by SIW for 60 GHz band," in IET Microwaves, Antennas & Propagation, vol. 10, no. 3, pp. 288-292, 19 2 2016.
[9] X. Zhuge and A. G. Yarovoy, "Study on Two-Dimensional Sparse MIMO UWB Arrays for High Resolution Near-Field Imaging," in IEEE Transactions on Antennas and Propagation, vol. 60, no. 9, pp. 4173-4182, Sept. 2012.
[10] Caratelli, D., and Viganó, M. C. (2011), Analytical synthesis technique for linear uniform-amplitude sparse arrays, Radio Sci., 46, RS4001
[11] Y. Aslan, J. Puskely, A. Roederer and A. Yarovoy, "Synthesis of multiple beam linear arrays with uniform amplitudes," 12th European Conference on Antennas and Propagation (EuCAP 2018), London, 2018, pp. 1-5.